ORIGINAL PAPER

An SHPB Test Study on Stress Wave Energy Attenuation in Jointed Rock Masses

J. C. Li[1,3] · L. F. Rong[1,2] · H. B. Li[1] · S. N. Hong[1,2]

Abstract

A series of dynamic tests were carried out to investigate the effect of joint roughness on the wave energy attenuation in rock masses and estimate the relation between joint roughness and seismic quality factor of rock masses. The modified split Hopkinson pressure bar (SHPB) apparatus was adopted in this study, where the loading, input and output bars were made of gypsum. The propagation coefficient of the gypsum bars was measured from trial tests. According to the propagation coefficient of the gypsum bars, the strain, stress and particle velocity on the contact surfaces between the specimen and input/output bars were obtained from the test data recorded by the strain gauges. The specimens were prepared by a three-dimensional printer with plaster and binder. Each specimen modeled a rock mass with one joint with different roughness. The seismic quality factor of specimen is also estimated from the proposed approach of wave energy dissipation. The effects of joint roughness on the seismic quality factor of rock mass and the wave energy attenuation across the rock mass are analyzed from test results.

Keywords SHPB test · Wave energy attenuation · Jointed rock mass · Joint roughness coefficient · Seismic quality factor

List of Symbols

Z_2	Root mean square of the first derivative of the profile curve
Δx	Scanning interval of points on the profile curve of joint surface
y_i	Vertical height of point on the profile curve of joint surface
m	Sampling number of the profile curve
D_s	Diameter of the specimen
l_s	Length of the specimen
$Q_{seismic}$	Seismic quality factor of rock mass
ΔW and W	Dissipation energy and maximum deformation energy of the specimen in one cycle of a harmonic excitation
σ	Stress on the specimen
ε	Strain of the specimen
$\dot{\varepsilon}$	Strain rate of the specimen
ε_{max}	Maximum value of strain
V_s	Volume of the specimen
W_I, W_R and W_T	Energies of incident, reflected and transmitted waves, respectively
W_S	Deformation energy of the specimen
t	Time
A and A_s	Cross-sectional area of the SHPB bars and specimen, respectively
ε_i, ε_r and ε_t	Strains caused by the incident, reflected and transmitted waves, respectively, on the input/output bar end contacted to the specimen
σ_i, σ_r and σ_t	Stress caused by the incident, reflected and transmitted waves, respectively, on the input/output bar end contacted to the specimen
ε_m, σ_m and v_m	Strain, stress and particle velocity caused by the waves on the interfaces between the specimen and input/output bars, respectively, and the subscript m is i, r or t for the incident, reflected and transmitted waves, respectively

✉ J. C. Li
jcli@whrsm.ac.cn

1. State Key Laboratory of Geomechanics and Geotechnical Engineering, Institute of Rock and Soil Mechanics, Chinese Academy of Sciences, Wuhan 430071, China

2. University of Chinese Academy of Science, Beijing 100049, China

3. School of Civil Engineering, Southeast University, Nanjing 210096, China

$\tilde{\varepsilon}_m$, $\tilde{\sigma}_m$ and $\tilde{v}_m$	Fourier forms of the strain, stress and particle velocity caused by the waves on the contact surfaces between the specimen and input/output bars, respectively, and the subscript m is i, r or t for the incident, reflected and transmitted waves, respectively
$\tilde{\varepsilon}'_m$	Fourier forms of strain due to the waves measured by the gauges on the input and output bars, and subscript m is i, r or t for the incident, reflected and transmitted waves, respectively
x	Distance of wave propagation from the strain gauges to the contact surface between the specimen and input/output bar
γ	Propagation coefficient of viscoelastic medium
α and k	Attenuation coefficient and wave number, respectively

1 Introduction

Joints widely exist in natural rock mass, which significantly affect the dynamic response of rock mass (Aydan 2017) and wave propagation across the rock mass. Plane stress waves generally attenuate during wave propagation across rock masses. The attenuation includes the frequency, amplitude and energy, which have received considerable attention and been applied to geology, geophysics, mining and earthquake engineering.

Stress wave attenuation in amplitude is closely related to the physical and mechanical properties of joint. Pyrak-Nolte et al. (1990) considered the joint as a displacement discontinuity and derived complete solutions for wave reflection and transmission across a joint. The solution indicates the amplitude of transmitted wave increases with the increase of stiffness of joint. Zhao et al. (2006), Perino et al. (2010), and Li (2013) studied linear and nonlinear parallel joints on wave transmission and reflection among a rock mass. Zhu et al. (2011) analyzed the influence of viscoelastic deformation behavior of filled joint on wave transmission, and the result revealed that the stiffness, viscosity and acoustic impedance of filled joint affect wave propagation. The above analytical results indicate that the properties of joint, such as the joint stiffness, spacing and filling material, have different influences on the amplitude and frequency of transmitted wave. In addition, the test study based on a split Hopkinson rock bar showed that the stiffness of filled joint affects wave attenuation (Wu et al. 2013). The study conducted by Fan and Wong (2013) shows that the unloading behavior of

joint greatly affects the amplitude and energy transmission of stress wave.

Stress wave energy attenuation in rocks can be attributed to two factors: intrinsic anelasticity of matrix minerals in rocks and frictional dissipation due to relative deformation of joints, and joints are considered to be the major factor (Johnston et al. 1979). Joints appear different deformation behaviors because of their various surfaces, which result in different attenuation degrees of stress wave. During various geological processes, joint surfaces may be altered, crushed and become rough. The contact and roughness of two surfaces of joint are two main geometrical factors to influence its mechanical property. Barton and Choubey (1977) presented a joint roughness coefficient (JRC) to describe the roughness of joint surfaces. Brown and Scholz (1986) studied the effect of rough and mismatched surfaces on joint closure by comparing experimental and theoretical results. Besides JRC, a surface geometrical parameter, i.e. joint matching coefficient (JMC), was coupled with JRC to fully describe the joint surface geometry and to estimate the mechanical properties of joints (Zhao 1997a, b). The modeling results of Hopkins (2000) indicate that the stiffness of joints depends on the overall spatial geometry of joint contact area, and the joint with contact area uniformly distributed across the surfaces is stiffer than that with non-uniformly distributed area.

Many studies have shown that the two geometrical parameters of joint, i.e. JMC and JRC, significantly affect wave attenuation. The quasi-static resonant column test to simulate long-wavelength wave propagation across rock masses (Mohd-Nordin et al. 2014) showed that under low normal stress, JRCs of joints have great influence on damping ratio of rock mass. The modified split Hopkinson pressure bar test conducted by Chen et al. (2015, 2016) showed that the wave transmission coefficient decreases nonlinearly with the JMC of joints. Meanwhile, the thickness and spatial geometry of contact area of joint also have effects on transmission coefficient. The similar results were revealed by the SHPB tests conducted on the joints with different JMCs (Li et al. 2017).

The seismic quality factor ($Q_{seismic}$) has been adopted widely to describe the seismic quality of rock mass and wave attenuation across it. The factor was defined as the ratio of the stored energy to the dissipation energy in one cycle of harmonic excitation in a certain volume of medium (Knopoff 1964). Pyrak-Nolte et al. (1990) carried out a series of ultrasonic tests on intact rock samples and jointed rock samples, and calculated $Q_{seismic}$ using spectral ratio method. The test results revealed that $Q_{seismic}$ increases with the increase of stiffness of joint. Because of the effects of JRC and JMC on wave attenuation, it can be surely deduced that $Q_{seismic}$ is closely related to JMC and JRC. However, the relation between JRC and $Q_{seismic}$ has not been well understood so far, due to lack of direct experiment data.

The intention of the present study is to investigate the effect of joint roughness on wave energy attenuation in rock masses and the relation between the joint roughness and the seismic quality factor of rock mass. A series of dynamic tests were carried out using a modified split Hopkinson pressure bar (SHPB) apparatus. Each specimen was composed of two contacted cylinders to model a rock mass with one joint. The specimens were prepared by a three-dimensional (3D) printer. The contact surfaces of two printed cylinders form artificial joints with different roughness. An approach based on wave energy dissipation is introduced to calculate $Q_{seismic}$ of specimens with different JRCs. Then, the effects of JRC on $Q_{seismic}$ of rock mass are analyzed and discussed.

2 SHPB Test

2.1 Specimen Preparation

In the test, each specimen was composed of two cylinders with the same diameter 50 mm, as shown in Fig. 1a. Each cylinder was around 15 mm long and the total length of the specimen is 30 mm. The two cylinders were contacted by two rough bottoms which modeled the interface of artificial rock joint in this study. The other bottom of each cylinder was smooth and flat and contacted to the input/output bar. The artificial joint roughness is the roughness of the interface.

Fig. 1 Specimens for SHPB test
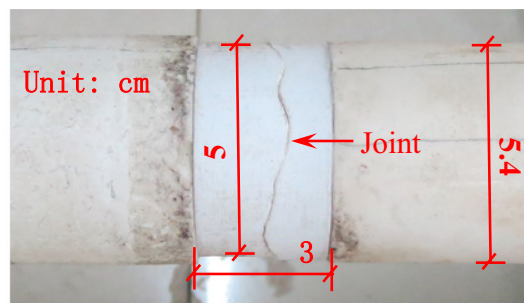
(a) Specimen with rough joint
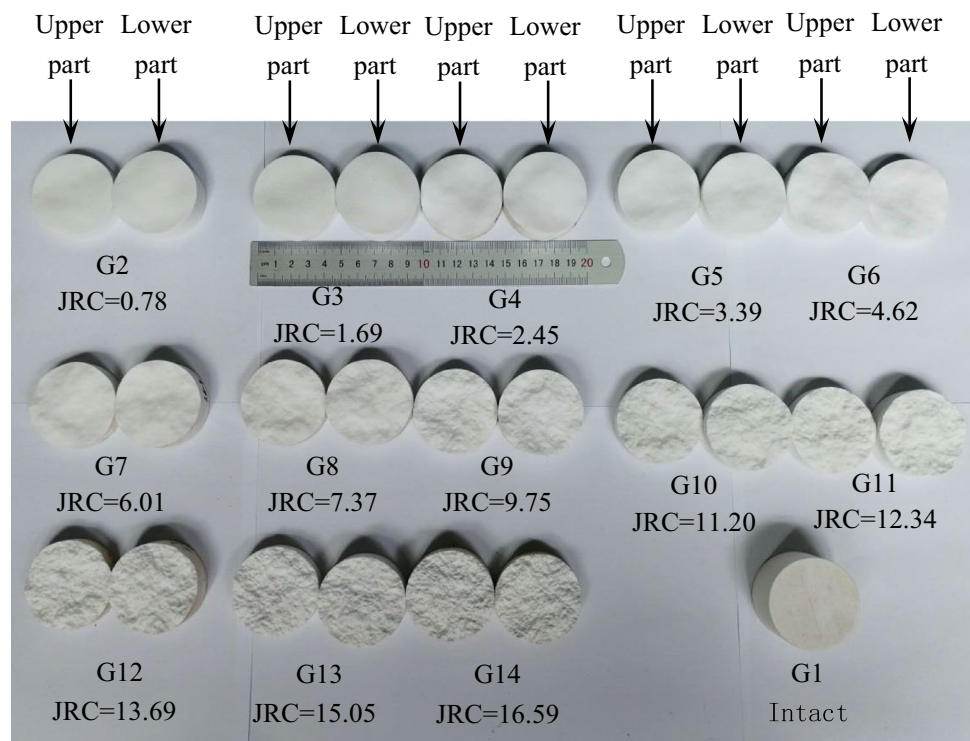
(b) 3D printed blocks with different rough surfaces

Artificial joints with a certain roughness can be made from two contacted surfaces using different methods, such as the rock stretch/splitting, the geomaterial pouring and 3D printing. The joint roughness coefficient (JRC) is random for natural joints or joints from stretch/splitting tests. To quantitatively study the effect of JRC on wave energy attenuation, the 3D printer (type of 3D Systems ProJet 260C) was adopted to prepare the specimens with different JRCs for joints. The printed specimens were made from gypsum plaster and binder. There were two steps to print the specimens: graphical model imaging and printing. The graphical model imaging was generated by the Geomagic Control, which is a supporting software of the 3D printer. The rough surface was formed by the software SynFrac (Ogilvie et al. 2006), where the surface roughness degree is decided by the power spectral density of surface morphology, $G(k)$, and a small value of $G(k)$ represents a smoother surface. The power spectral density is correlated with an input parameter, i.e. fractal dimension of surface, D, and the relation is described as (Brown 1995)

$$G(k) = Ck^{-(7-2D)}, \tag{1}$$

where $k = 2\pi/\lambda$, and λ is the length of wave describing the surface morphology; C is the proportionality constant. As shown in Eq. (1), $G(k)$ increases with the increase of D, which means the surface becomes rougher.

The original graphical model was an intact cylinder and then cut into two subcylindrical blocks with the same height using one rough surface on the middle position of the cylinder axis. Hence, the new graphical model was composed of two parts: the upper and lower blocks. The two parts have the same cross-section and almost the same height. For each subcylindrical block, one bottom was rough, while the other was smooth and flat. The rough bottoms of two blocks were the same and contacted with each other. The rough bottom became rougher when a big value of the input parameter, i.e. fractal dimension D, was chosen. Then, the new graphical model was sent into the 3D printer, and the specimen with two blocks was printed out subsequently. When the input fractal dimension was changed, the specimens with different rough joints were produced. Figure 1b shows the printed blocks with different rough surfaces.

Because of the limit of the print accuracy of 3D printer (0.1 mm), the surface morphology of specimen printed is a little different to the graphical model designed. To accurately measure the rough surface morphology of specimen, the 3D scanner (type of Geomagic Capture) was used to scan the rough surface of the printed cylinders to obtain the more precise 3D digital images. Figure 2 shows 12 scan lines through the circle center were uniformly distributed on the rough surface. From the scan lines, 12 profile curves were extracted in the range of the cylinder diameter. To some extent, the geometrical characteristics of rough surface can be described from the 12 profile curves, which were used to calculate the JRC of each joint before the test. The 12 scanned curves for a rough surface were set a group here.

If each profile curve presents a two-dimensional (2D) problem, the JRC^{2D} can be calculated from a commonly adopted empirical equation (Yang et al. 2001):

$$JRC^{2D} = 32.69 + 32.98\log_{10}Z_2, \tag{2}$$

where the parameter Z_2 is given as

$$Z_2 = \left[\frac{1}{m(\Delta x)^2} \sum_{i=1}^{m} (y_{i+1} - y_i)^2\right]^{1/2}, \tag{3}$$

the symbol Δx denotes the sampling interval of points on one profile curve, and Δx is 0.25 mm in this study; the form '$y_{i+1} - y_i$' denotes the vertical difference between two adjacent points along the profile curve; and the symbol m denotes the sampling number on the profile curve and is related to the ratio of cylindrical diameter D_s and point sampling interval Δx, that is, $m = 1 + \text{integer}(D_s/\Delta x)$.

Fig. 2 Joint surface digital image and the scan line
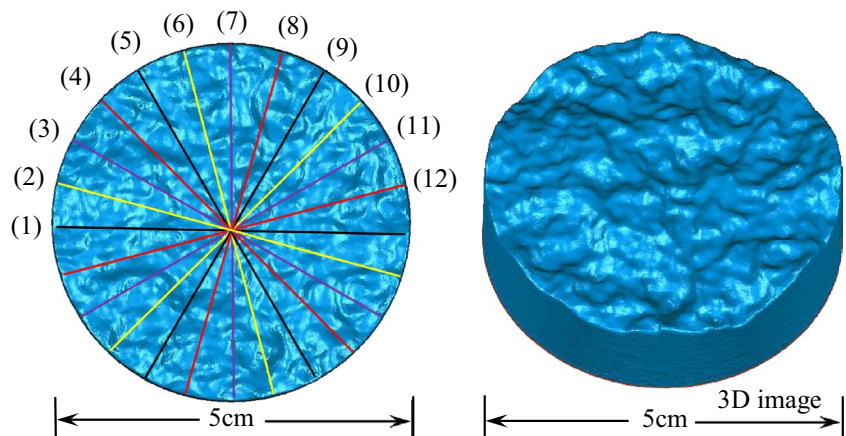
The JRC of rough surface can be considered as the average value of the JRC^{2D} of the 12 profile curves shown in Fig. 2, i.e.

$$JRC = \frac{1}{12} \sum_{i=1}^{12} (JRC^{2D})_i. \tag{4}$$

In this equation, $(JRC^{2D})_i$ represents the rough degree of profile line and obtained from Eq. (1). JRC shows the roughness degree of surface. When a fractal parameter is chosen for a rough surface of 3D printing model, the JRC of the rough joint can be calculated from Eq. (3). The fractal parameters ranging from 0.5 to 2.5 were chosen and the subcylindrical blocks with different roughness coefficients ranging from 0.78 to 16.59 were printed, as shown in Fig. 1b. Each specimen was composed of the upper and lower blocks with the same JRC. Table 1 shows the parameters of the 14 printed specimens when JRC ranges from 0 to 16.59. The specimen G1 is an intact gypsum cylinder without joint, that is, JRC for G1 is zero. The height of the specimen G1 is 30 mm. The printed specimens were used for the SHPB test, as shown in Fig. 1.

In addition, four intact specimens with diameter 50 mm and length 100 mm were printed by the 3D printer to obtain the basic physical parameters of specimen, such as the density and wave propagation velocity. The density and longitudinal wave velocity of the intact specimens were measured to be 1300 kg m^{-3} and 1820 m s^{-1}, respectively.

Table 1 The parameters of the jointed specimens with different JRCs

| Series number	Diameter	Length	Input parameter Fractal dimension	JRC
G1	50 mm	30 mm	–	0.00
G2			0.5	0.78
G3			0.8	1.69
G4			1.00	2.45
G5			1.20	3.39
G6			1.40	4.62
G7			1.60	6.01
G8			1.80	7.37
G9			2.00	9.75
G10			2.10	11.20
G11			2.20	12.34
G12			2.30	13.69
G13			2.40	15.05
G14			2.50	16.59

2.2 Experimental Setup

The steel bars are commonly used as the input and output bars in the traditional SHPB apparatus. The impedance of steel bars is larger and almost 16 times than that of the printed specimens. The impedance of the printed specimens is about 2,366,000 kg m^{-2} s^{-1}, while the impedance of steel bars is about 39,936,000 kg m^{-2} s^{-1}. The difference between the impedances of input/output bars and specimens is so large that the stress wave hardly transmits across specimen. When the traditional SHPB apparatus is adopted to carry out dynamic test on the printed specimens, the amplitude of stress wave in output bar is too low to measure precisely. Hence, the low impedance bars, i.e. gypsum bars were chosen to replace the steel bars in SHPB apparatus to carry out dynamic tests on the printed specimens in this study.

The dynamic test was conducted using a modified split Hopkinson pressure bar (SHPB) apparatus, as shown in Fig. 3. The apparatus consists of a dynamic loading device, an input bar, a specimen, an output bar and a data acquisition unit. Having the same cylindrical cross-section with diameter 54 mm, the striker, input and output bars measure 100, 1000 and 1000 mm in length, respectively. The three bars are made of gypsum. During the preparation of the bars, a certain amount of gypsum powder was first mixed with water by the ratio of 3:1, and then the mixture was poured into the plastic molds, which were a hollow cylinder with 54 mm in inner diameter. After 1-month maintenance at room temperature, the bars were solidified. The two ends of each bar were ground to ensure them flat before the test. The density ρ and Young's modulus E of the gypsum bars are 1708 kg m^{-3} and 15.4 GPa, respectively, while the uniaxial compression strength of the gypsum bars is 54 MPa. The data acquisition unit included two groups of strain gauges, a dynamic strain meter and an oscilloscope. Each group of strain gauges was stuck on the input/output bars. A specimen was sandwiched between the input and output bars.

2.3 Test Proceeding

A series of impact tests on the jointed specimens were conducted using the modified SHPB apparatus. Before the tests, a specimen was sandwiched between the input and output bars, and an appropriate amount of Vaseline was painted on the contact surfaces between the specimen and input/output bar to reduce the frictional effect. The impact velocity of the loading bar was controlled to be around 0.5 m s^{-1} to avoid damage in the bars and specimens. High loading rates are usually generated from an explosive excavation. So we chose the impact velocity of loading bar to simulate the load induced by explosive excavations. The test for each specimen was conducted repeatedly three times under the same loading condition to ensure the test result reliable. The

Fig. 3 Modified SHPB test
equipment
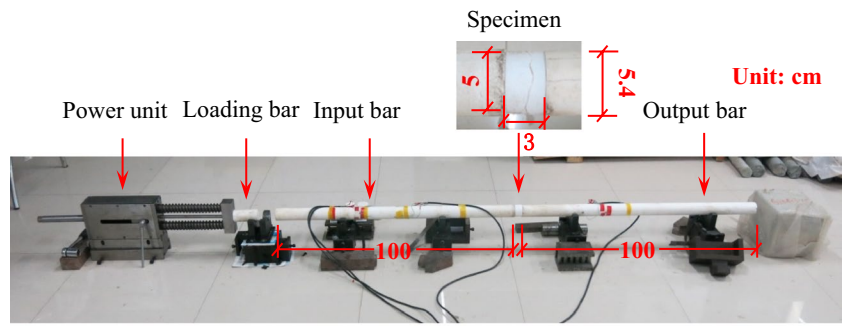
(a) Modified Split Hopkinson Pressure Bar (SHPB) test equipment
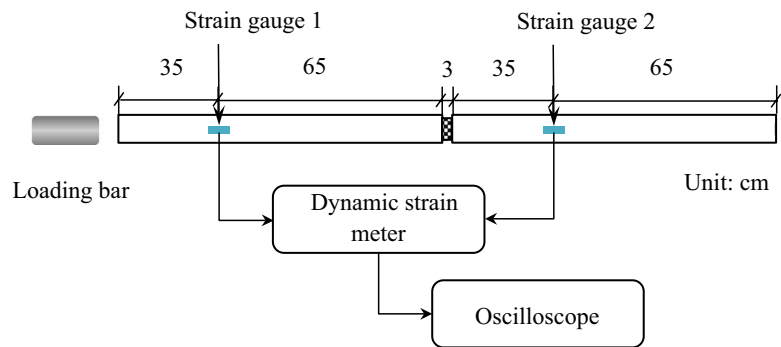
(b) Schematic view of modified SHPB test equipment

velocity of longitudinal wave in the gypsum bars was measured about 3200 m s^{-1}.

During the tests, launched by the dynamic loading device, a loading bar impacted on the input bar and consequently the incident wave was generated and propagated along the input bar. When the incident wave arrived at the interface between the input bar and the specimen, reflected wave was caused from the interface and propagated along the input bar in the opposite direction of incident wave. Meanwhile, the specimen deformed. At this moment, the transmitted wave was generated on the interface between the specimen and output bar and propagated along the output bar. The waves, named as incident, reflected and transmitted waves, respectively, were measured by strain gauges glued on the input and output bars, and then collected by the dynamic strain meter and stored by the oscilloscope.

3 Estimation of Q_{seismic}

3.1 Approaches to Calculate Q_{seismic}

The seismic quality factor, denoted as Q_{seismic}, is commonly used to indicate seismic wave energy attenuation in a rock mass and defined as the ratio of stored energy to dissipation energy (Knopoff 1964),

$$2\pi/Q_{\text{seismic}} = \Delta W/W, \tag{5}$$

where the symbol ΔW denotes the dissipated energy in one cycle of a harmonic excitation, and the symbol W denotes the maximum deformation deformation energy stored in the medium. The right part of Eq. (5), i.e. $\Delta W/W$, can be considered as the loss rate of energy (Kolsky 1963). The cycle
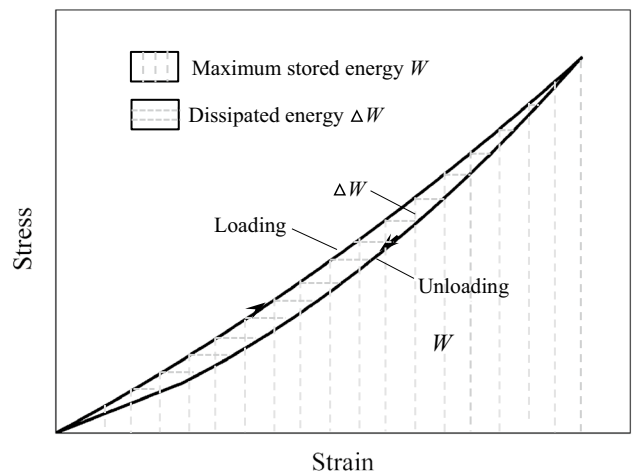

Fig. 4 Calculation of Q_{seismic} based on the relationship between stress–strain curve

of excitation is the loading and unloading paths caused by the stress wave propagation across the medium. Hence, the seismic quality factor of rock mass, Q_{seismic}, can be estimated from the deformation energy of medium. Figure 4 is the schematic view of Q_{seismic} calculated from the deformation energy of specimen. The dissipated energy ΔW and the maximum value of deformation energy W can be obtained by integrating the stress over strain from the stress vs strain curve, that is,

$$\Delta W = V_s \oint \sigma \mathrm{d}\varepsilon, \tag{6a}$$

$$W = V_s \int_0^{\varepsilon_{\max}} \sigma \mathrm{d}\varepsilon, \tag{6b}$$

where σ denotes the stress on the specimen; the symbol ε denotes the strain of the specimen; $\varepsilon_{\max}$ is the maximum value of strain; and V_s is the volume of the specimen.

The above approach is from the definition of Q_{seismic} and is based on the stress–strain curve of specimen (called stress–strain approach). Since the dynamic stress–strain relation of specimen is estimated from SHPB tests, the seismic quality factor Q_{seismic} may also be calculated from the stress waves propagating across the specimen.

During the SHPB test, when the incident wave arrives at and propagates across the specimen, the reflected and transmitted waves generated from the specimen-bar interfaces begin to propagate along the input and output bars, respectively. The specimen deforms consequently. Here, the loss of energy caused by friction in the apparatus is omitted. Induced by the impact of loading bar, the energy of incident wave is assumed to completely transform into the energies of reflected and transmitted waves and the work on the specimen according to the energy conservation. Hence, the work on the specimen, denoted as U, can be expressed as

$$U = W_{\text{I}} - W_{\text{R}} - W_{\text{T}}, \tag{7}$$

where W_{I} denotes the energy of incident wave; W_{R} and W_{T} denote the energies of reflected and transmitted waves, respectively.

The test apparatus is considered to be isolated. According to the first law of thermodynamics, the work on the specimen U is equal to the deformation energy of the specimen W_{S}, that is,

$$W_{\text{S}} = U = W_{\text{I}} - W_{\text{R}} - W_{\text{T}}. \tag{8}$$

During the test, the wave energy and the deformation energy of specimen are time related, so Eq. (8) can be rewritten as

$$W_{\text{S}}(t) = W_{\text{I}}(t) - W_{\text{R}}(t) - W_{\text{T}}(t) \quad (0 \leqslant t \leqslant t_0), \tag{9}$$

where t_0 denotes the loading duration.

Based on the elastic theory, the energies of stress waves propagated in the input and output bars, W_{I}, W_{R} and W_{T}, can be estimated from the stress and strain of the bars, i.e.

$$W_{\text{I}} = Ac \int_0^t \sigma_i(t)\varepsilon_i(t)\mathrm{d}t$$

$$W_{\text{R}} = Ac \int_0^t \sigma_r(t)\varepsilon_r(t)\mathrm{d}t \tag{10}$$

$$W_{\text{T}} = Ac \int_0^t \sigma_t(t)\varepsilon_t(t)\mathrm{d}t,$$

where A denotes the cross-sectional area of the two bars; $\varepsilon_i(t)$, $\varepsilon_r(t)$ and $\varepsilon_t(t)$ denote the strains of the bars caused by the incident, reflected and transmitted waves, respectively; and $\sigma_i(t)$, $\sigma_r(t)$ and $\sigma_t(t)$ denote the stresses on the bars caused by the incident, reflected and transmitted waves, respectively; and c is the speed of the longitudinal wave propagating in the gypsum bars.

Substituting Eq. (10) into Eq. (9), there is

$$W_{\text{S}}(t) = Ac \int_0^t \left(\sigma_i(t)\varepsilon_i(t) - \sigma_r(t)\varepsilon_r(t) - \sigma_t(t)\varepsilon_t(t) \right)\mathrm{d}t. \tag{11}$$

The difference between the total energy of incident wave and the sum of the total energies of reflected and transmitted waves is the amount of dissipated energy of the stress waves ΔW, which is equal to the value of deformation energy of specimen $W_{\text{S}}(t_0)$ at the final time t_0. Then, ΔW can be rewritten as

$$\Delta W = W_{\text{S}}(t_0) = Ac \int_0^{t_0} \left(\sigma_i(t)\varepsilon_i(t) - \sigma_r(t)\varepsilon_r(t) - \sigma_t(t)\varepsilon_t(t) \right)\mathrm{d}t. \tag{12}$$

The maximum stored energy W, i.e. the maximum value of the deformation energy of specimen, is caused by the three waves and can be rewritten as

$$W = \max\left(Ac \int_0^t \left(\sigma_i(t)\varepsilon_i(t) - \sigma_r(t)\varepsilon_r(t) - \sigma_t(t)\varepsilon_t(t) \right)\mathrm{d}t \right). \tag{13}$$

When Eqs. (12) and (13) are substituted into Eq. (5), the seismic quality factor Q_{seismic} can be expressed as another form based on the stress wave energy, that is,

$$Q_{\text{seismic}} = 2\pi \frac{\max\left(\int_0^t \left(\sigma_i(t)\varepsilon_i(t) - \sigma_r(t)\varepsilon_r(t) - \sigma_t(t)\varepsilon_t(t) \right)\mathrm{d}t \right)}{\int_0^{t_0} \left(\sigma_i(t)\varepsilon_i(t) - \sigma_r(t)\varepsilon_r(t) - \sigma_t(t)\varepsilon_t(t) \right)\mathrm{d}t}. \tag{14}$$

In this section, there are two approaches to estimate the seismic quality factor: one is based on the stress–strain curve of specimen (called stress–strain approach) and another is based on the energies of stress waves in the input/output bars (called wave energy approach). In SHPB tests, the

latter approach is more convenient to calculate the value of Q_{seismic} than the former one. The waves propagating in the input/output bars can be measured directly in the SHPB tests, and the wave data are directly used to calculate Q_{seismic} based on the wave energy approach. The former approach is a traditional method introduced by Kolsky (1963), which depends on the stress–strain curve of specimen. If the former approach is adopted, the dynamic stress–strain curve of specimen must be obtained first from the time histories of stress and strain, which are calculated from the test data. The dissipated energy ΔW and the maximum value of deformation energy W are then obtained by integrating the dynamic stress–strain curve to calculate the value of Q_{seismic}. Therefore, the stress–strain approach is some complex, while the wave energy approach is easy and can be used directly from the test data. In this study, the wave energy approach was adopted to calculate the seismic quality factor of a specimen with one joint from SHPB test data.

3.2 Test Data Process

The gypsum bars of the modified SHPB apparatus are imperfectly elastic but still might cause amplitude and frequency attenuations of wave due to the existence of various inherent micro-defects. The gypsum bars are hence assumed to be viscoelastic in this study. In the conventional SHPB test, there is no wave attenuation along the elastic metal bar and the waves at different positions on the bar have the same waveform with phase difference. Unlike the conventional SHPB test, the stress wave attenuates along the gypsum bars in the modified SHPB test, which causes the stress wave on the contact interface between the specimen and the input/output bars different from the stress wave at any other location of the bar. It should be noted that the incident, reflected and transmitted waves applied in the proposed approach of Sect. 3.1 are the stress waves on the contact surfaces between the specimen and input/output bars. Bacon (1998) suggested a propagation coefficient γ for wave attenuation in a viscoelastic medium, that is,

$$\gamma^2 = -\frac{\rho\omega^2}{E^*}, \tag{15}$$

where E^* denotes the viscoelastic modulus of gypsum; ω denotes the angular frequency, $\omega = 2\pi f$, and f is the frequency. The propagation coefficient γ is a complex number and expressed as

$$\gamma(\omega) = \alpha(\omega) + ik(\omega), \tag{16}$$

where $\alpha(\omega)$ denotes an attenuation coefficient, and $k(\omega)$ denotes the wave number.

The propagation coefficient γ is adopted in this study to get the stress waves on the contact surfaces between the specimen and the input/output bars. To obtain the
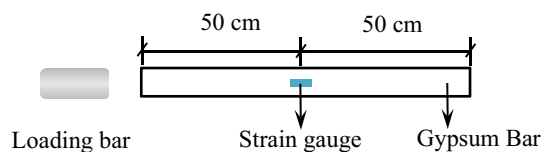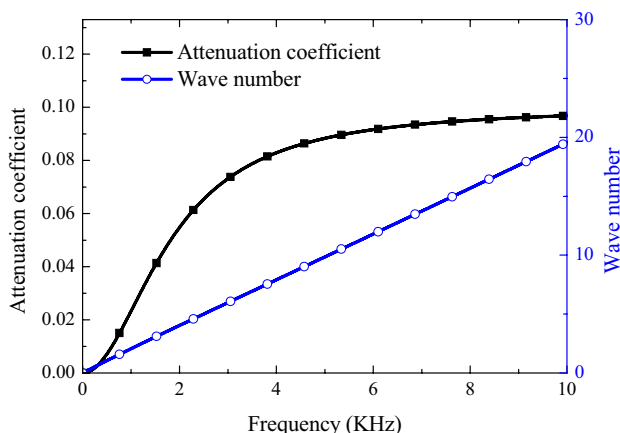

Fig. 5 Schematic view of the trial test

Fig. 6 The two components of wave propagation coefficient γ of gypsum bar

propagation coefficient of the gypsum bar, a trail test was carried out to study the viscoelastic property of the gypsum bar.

The trail test included a loading and gypsum bars. The later one was the input/output bar of the modified SHPB, as shown in Fig. 5. In the trail test, a stress pulse was generated when one end of the bar was impacted by the loading bar while the other end of the bar was free. A strain gauge was glued at the middle position of bar to record the incident and reflected strain waves propagating in the bar.

From the definition of propagation coefficient (Bacon 1998), there is

$$e^{-\gamma 2d} = -\frac{\tilde{\varepsilon}_i'(\omega)}{\tilde{\varepsilon}_r'(\omega)}, \tag{17}$$

where $\tilde{\varepsilon}_i'(\omega)$ and $\tilde{\varepsilon}_r'(\omega)$ are the Fourier transforms of incident wave $\varepsilon_i'(\omega)$ and the reflected wave $\varepsilon_r'(\omega)$ measured by the gauges on the gypsum bar, respectively; d denotes one-half length of gypsum bar, and $d = 0.5$ m. The propagation coefficient γ can then be obtained from Eq. (17) according to the incident and reflected strain waves recorded in the trail test. The result of the trail test is shown in Fig. 6.

Based on the general solution of one-dimensional equation of axial motion of viscoelastic bar (Bacon 1998), the strain, stress and particle velocity on the contact surfaces

Fig. 7 The calculation process of the seismic quality factor by two approaches
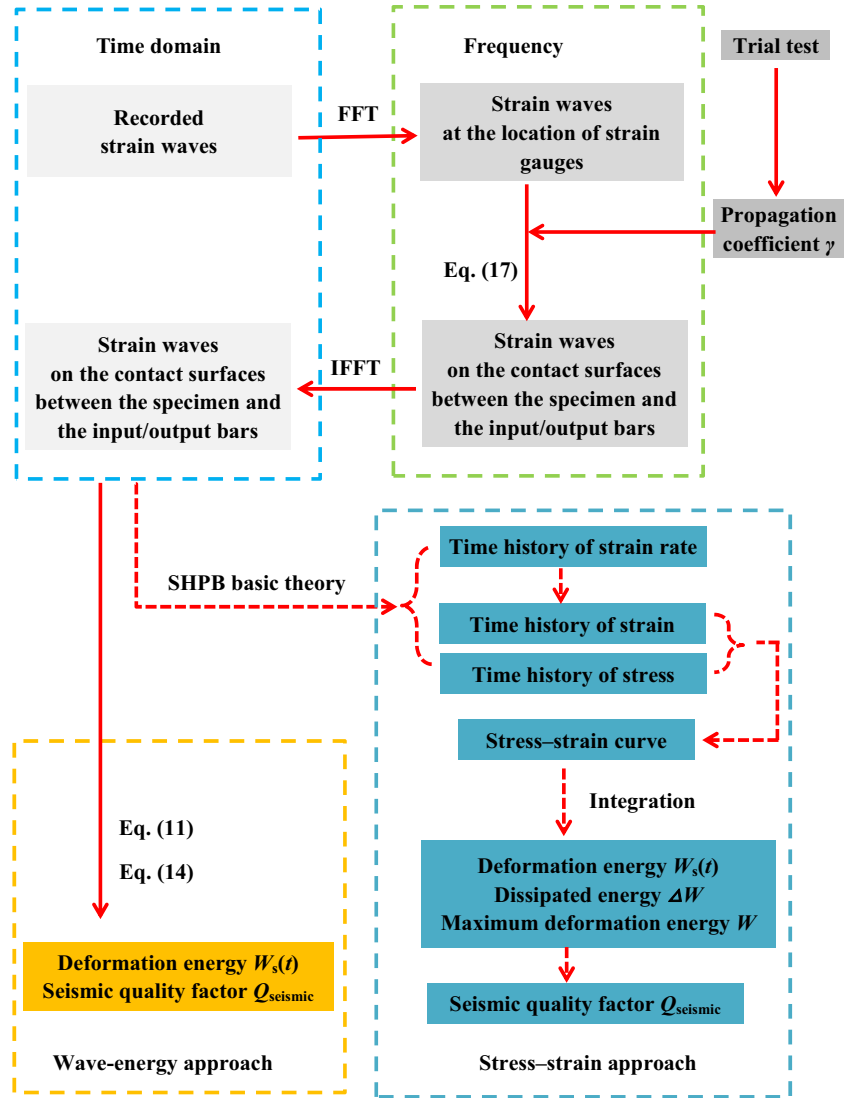
Note: The strain waves are incident, reflected and transmitted wave, respectively.

between the specimen and input/output bars can be calculated after the Fourier transformation, that is,

$$\tilde{\varepsilon}_m(\omega) = \tilde{\varepsilon}'_m(\omega)e^{-\gamma x}, \tag{18a}$$

$$\tilde{\sigma}_m(\omega) = -\frac{\rho\omega^2}{\gamma^2}\tilde{\varepsilon}'_m(\omega)e^{-\gamma x}, \tag{18b}$$

$$\tilde{v}_m(\omega) = -\frac{i\omega}{\gamma}\tilde{\varepsilon}'_m(\omega)e^{-\gamma x}, \tag{18c}$$

where $\tilde{\varepsilon}'_m(\omega)$ represents the Fourier forms of strain measured by the gauges on the input and output bars; $\tilde{\varepsilon}_m(\omega)$, $\tilde{\sigma}_m(\omega)$ and $\tilde{v}_m(\omega)$ represent the Fourier forms of the strain, stress and particle velocity on the contact surfaces between the specimen and input/output bars, respectively. The subscript m is i, r or t for the incident, reflected or transmitted waves, respectively. The symbol x denotes the distance of wave

propagation from the strain gauge to the contact surfaces between the specimen and the input/output bars. And, x equals to 65 mm, -65 mm and -35 mm for the incident, reflected and transmitted waves, respectively.

On the contact surface, the strain $\varepsilon_m(t)$, stress $\sigma_m(t)$ and particle velocity $v_m(t)$ can be obtained from

$$\begin{cases} \varepsilon_m(t) = F^{-1}(\tilde{\varepsilon}_m(\omega)) \\ \sigma_m(t) = F^{-1}(\tilde{\sigma}_m(\omega)) \\ v_m(t) = F^{-1}(\tilde{v}_m(\omega)), \end{cases} \tag{19}$$

where F^{-1} is the function of inverse Fourier transform; the subscript m is i, r or t for the incident, reflected or transmitted waves, respectively.

When the stress, strain and velocity on the contact surfaces between the specimen and the bars are obtained, the

corresponding energies of the stress waves can be calculated from Eq. (10), so to calculate the work on the specimen. In addition, the deformation energy of specimen can be obtained from Eq. (11). According to the work on the specimen and the deformation energy of specimen, the seismic quality factor can be estimated from Eq. (14). For the sake of clarity, the calculation process of seismic quality factor is shown as Fig. 7.

Figure 7 illustrates that in the stress–strain approach, the stress vs strain curve of specimen could be used only after the time histories of stress on the specimen, strain rate and strain of the specimen are obtained from the waves on the interfaces between the specimen and input/output bars. Compared to the stress–strain approach, the process of the wave energy approach is simply and can be used directly from the waves to calculate the seismic quality factor of the specimen. In the next section, the calibration of the wave energy approach is done by comparing with the result from the stress–strain approach.

3.3 Comparison Between the Calculating Approaches of $Q_{seismic}$

In Sect. 3.1, two approaches to calculated $Q_{seismic}$ are introduced, one is based on the stress wave energy (called as wave energy approach) and the other is based on stress–strain curve of specimen (called as stress–strain approach). The second approach is a traditional method to calculate $Q_{seismic}$, which is used to prove the validity of the wave–energy approach in this section.
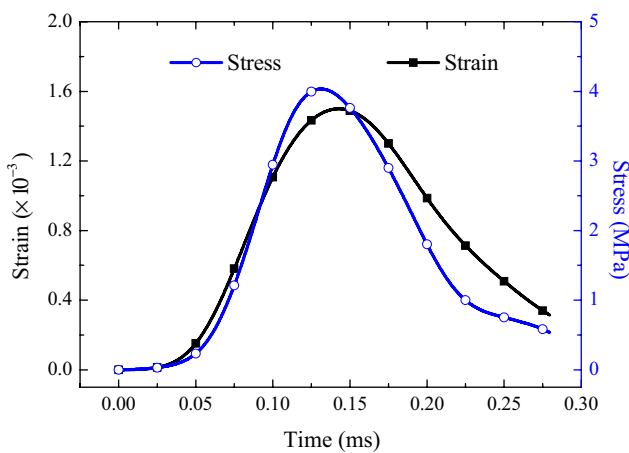
The intact gypsum specimen G1 was adopted to do the comparison between two approaches. Figure 8a shows
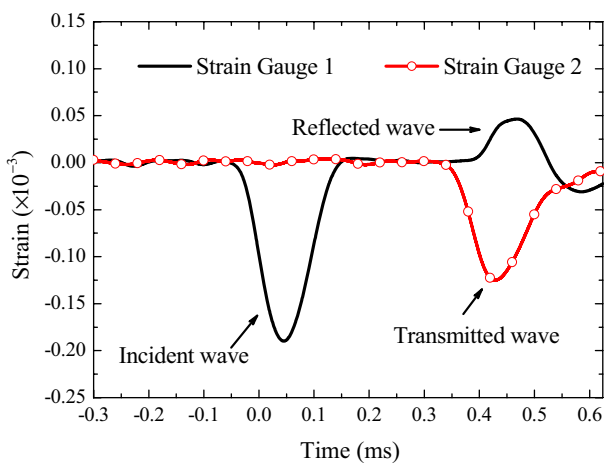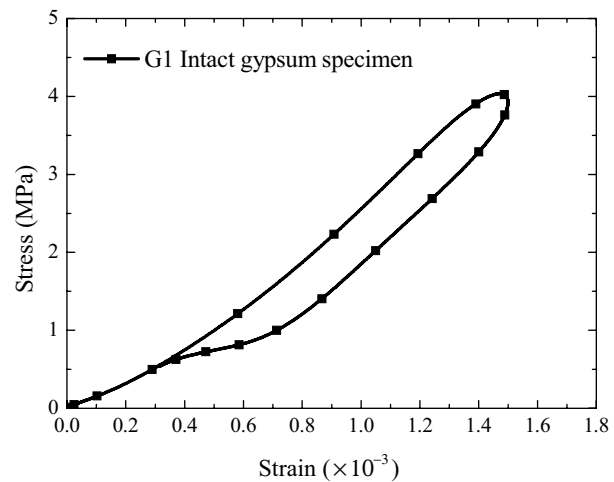

(a) Typical test data recorded by two strain gauges
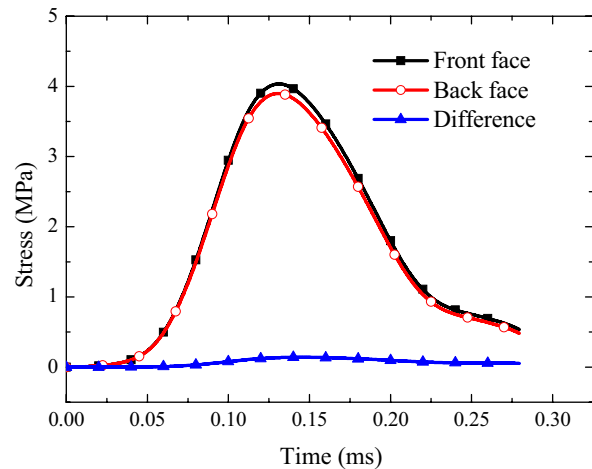
(b) Stresses on the front and back faces of specimen

(c) Strain and stress on the specimen

(d) Relationship between stress and strain of the specimen

Fig. 8 The stress and strain on the intact gypsum specimen G1

the waveforms from the test data, where the incident and reflected wave were recorded by strain gauge 1 glued on the input bar, while the transmitted wave was recorded by strain gauge 2 glued on the output bar. The location of the strain gauges is shown in Fig. 3b.

Based on 1D elastic wave theory, the stresses and velocities are calculated from test records shown in Fig. 8a, i.e. the incident, reflected and transmitted waves, respectively. The stresses, σ_i, σ_r and σ_t, and velocities, v_i, v_r and v_t, caused by the three elemental waves and acted on the interface of the specimen and input/output bars can then be separately obtained from Eqs. (18a, b, c) and (19).

The stress on the front face of the specimen contacted to the input bar is equal to the sum of stresses σ_i and σ_r, and the stress on the back face of the specimen contacted to the output bar is equal to the stress σ_t. The stresses on the front and back faces of the specimen are shown in Fig. 8b. It is found that both of the loading and unloading paths of stress are very close. The discrepancy appears around the maximum stress. In Fig. 8b, the maximum stress on the front face of the specimen is 4.04 MPa, while the maximum stress on the back face of the specimen is 3.89 MPa. The relative difference between the maximum stresses on the front and back face of the specimens is about 0.38%. Therefore, the stress on the specimen can be considered to be uniform.

From the fundamental theory of SHPB test, the stress σ, strain rate $\dot{\varepsilon}$ and strain ε of the specimen can be calculated from

$$\sigma(t) = \frac{A}{2A_s}\left(\sigma_i(t) + \sigma_r(t) + \sigma_t(t)\right), \tag{20a}$$

$$\dot{\varepsilon}(t) = \frac{1}{l_s}\left(v_i(t) - v_r(t) - v_t(t)\right), \tag{20b}$$

$$\varepsilon(t) = \frac{1}{l_s}\int_0^t \left(v_i(t) - v_r(t) - v_t(t)\right)dt, \tag{20c}$$

where A_s represents the cross-sectional area of the specimen, and l_s is the length of the specimen.

Figure 8c shows the time histories of stress on the specimen and strain of the specimen. The relation between these two physical variables is shown in Fig. 8d. The form of stress–strain curve shown in Fig. 8d is similar to that shown in Fig. 4, where the hysteresis loop means the deformation of specimen or the dissipation of input energy. The deformation energy of the specimen can be calculated by integrating stress over strain. The dissipation energy ΔW and the maximum stored energy W can be obtained from the stress–strain approach expressed as Eq. (6a, b). Meanwhile, the deformation energy also can be obtained from the wave energy approach expressed as Eq. (11).

Figure 9 shows the calculated results based on two approaches. It can be observed from the figure that the deformation energy of specimen calculated from the wave energy approach is quite similar to that calculated from the stress–strain approach. In the process of dynamic compression, the deformation energy of the specimen first increases, reaches the maximum value W, and then decreases to the residual deformation energy which is equal to the dissipation energy ΔW done by the stress waves. In Fig. 9, the maximum deformation energy W from the wave energy approach is 0.168 J and W from the stress–strain approach is 0.165 J. The discrepancy between the two energies is about 0.02%, which indicates that the work done by the stress wave is almost transformed into the internal energy of the specimen and causes the specimen to deform. The dissipation energy ΔW obtained from the wave energy approach is 0.037 J, while that obtained from the stress–strain approach is 0.042 J. The discrepancy between the dissipation energy is about 11.90%. Substituting the value of ΔW and W into Eq. (5), the seismic quality factors $Q_{seismic}$ are calculated to be 28.51 and 24.67 from the two approaches, respectively. The discrepancy of $Q_{seismic}$ between the two approaches is about 13.46%. The plot reveals that both of the deformation energy and $Q_{seismic}$ from the wave energy approach is very close to those from the stress–strain approach. From above, the wave energy approach is approved to be effective to calculate $Q_{seismic}$.

4 Test Result

Figure 10 shows the incident, reflected and transmitted strain waves recorded by the strain gauges for the specimens G4, G5, G7, G9, G12 and G13, with the JRCs of 2.65, 3.39, 6.01, 9.75, 13.69 and 15.05, respectively. The waveforms are basically the same although the JRCs of specimen are different.
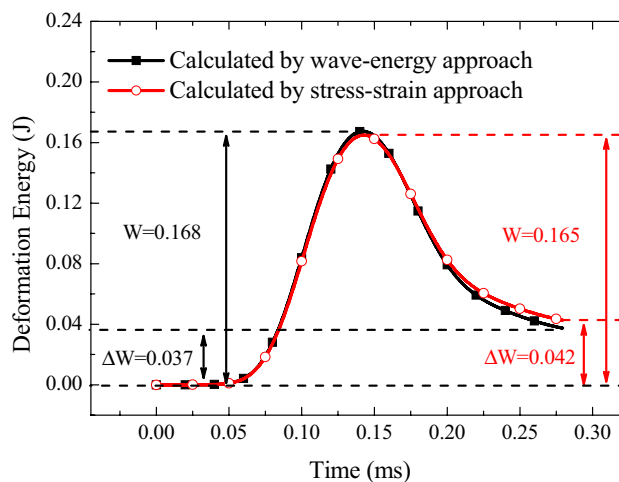

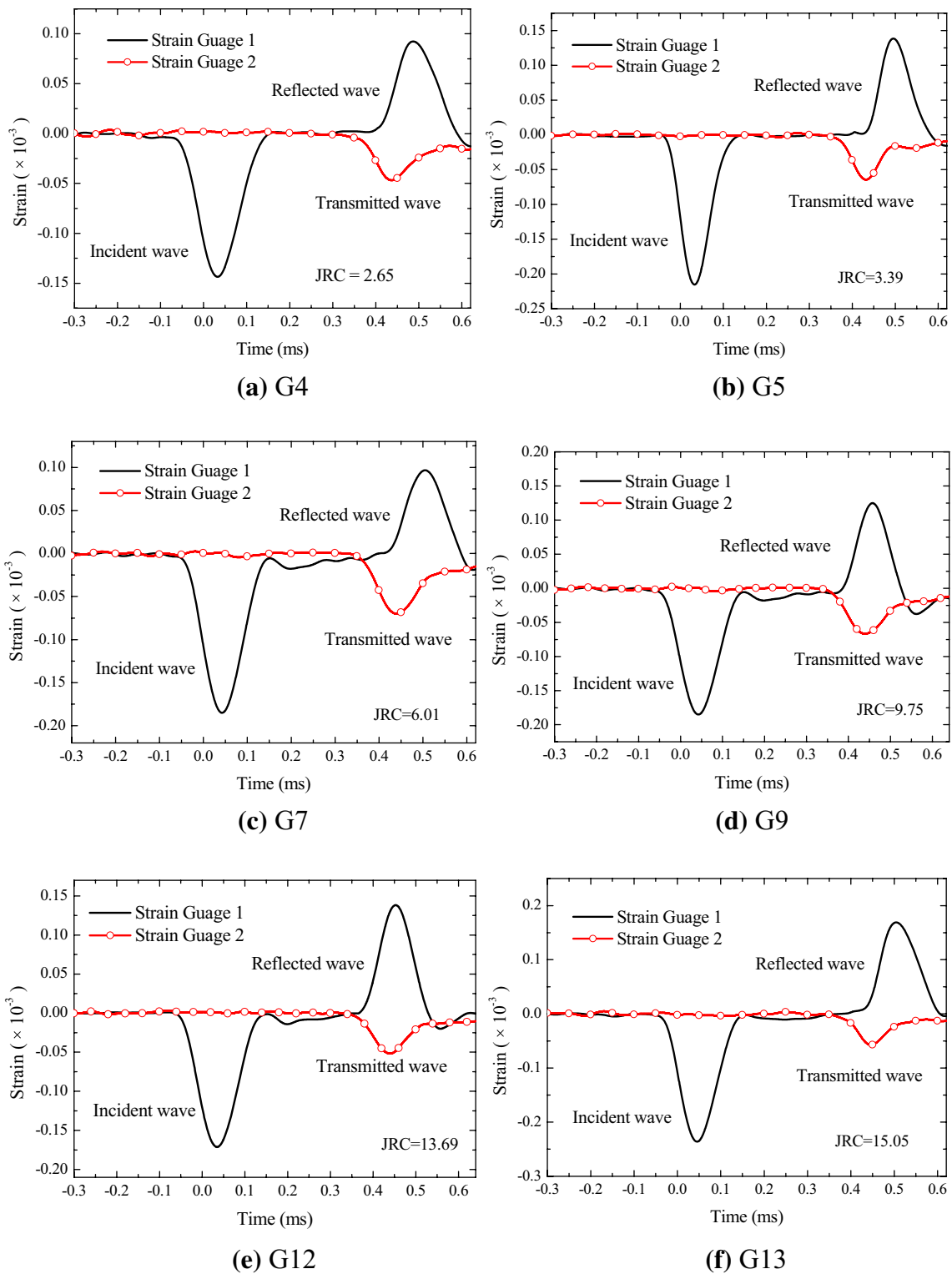**Fig. 9** Deformation energy of specimen based on two approaches

Fig. 10 The typical waveforms recorded by strain gauges

Among the three kinds of elemental waves, the amplitude of the incident wave is the greatest, and the amplitude of the transmitted wave is the smallest. It is different for the intact specimen G1 shown in Fig. 8a, where the amplitude of transmitted wave is obviously greater than that of the reflected wave. The difference between the intact specimen G1 and
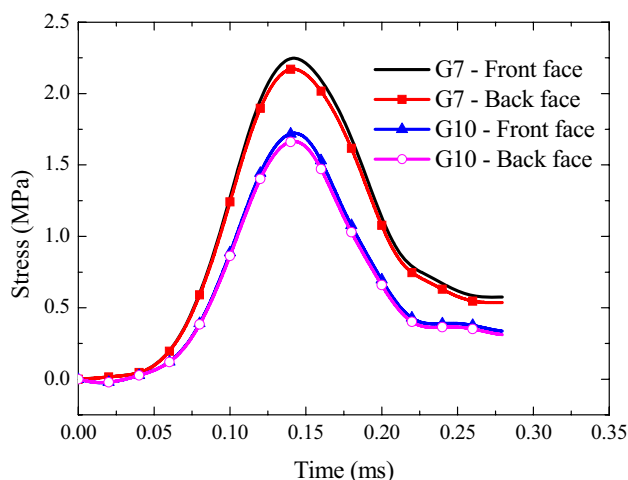
Fig. 11 Stress on specimens

the jointed specimens G4, G5 G7, G9, G12 and G13 is the existence of joint or, strictly speaking, the joint roughness coefficient. Hence, it can be deduced that the transmitted and reflected waves are related to the joint roughness coefficient.

The stresses on two faces of the specimens G7 and G10 are shown in Fig. 11. It is found that the stresses have a similar trend with variation of time, which increases first to a maximum value and then decrease. The maximum value of the stress is about 2.21 MPa for JRC being 9.75, and 1.69 MPa for JRC being 13.69.

The deformation energy for the jointed specimens with different JRCs was calculated from the stress wave data using wave energy approach. Figure 12 shows that the deformation energy varies with time for the six jointed specimens with JRCs being 2.65, 3.39, 6.01, 9.75, 13.69 and 15.05, respectively. It can be seen from the plot that the tendencies of deformation energy for six specimens are very similar, that is, the deformation energy increases sharply to a maximum value first and then decreases smoothly with the time going. The maximum stored energy, W, and the dissipation energy, ΔW, can be obtained from the deformation energy varying with time, which are the maximum value of the deformation energy and the final residual value of the deformation energy, respectively. As shown in the plot, both the maximum values and the final residual values of deformation energies are different when the JRCs of the specimens change. In another word, either the maximum deformation energy, W or the dissipated energy, ΔW, are different for the jointed specimens with different JRCs. And all the values of the maximum deformation energy, W, and the dissipation energy, ΔW for the specimens are listed in Table 2.
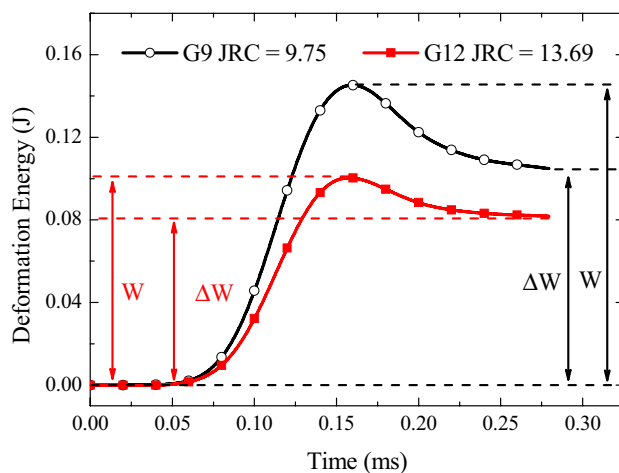
The seismic quality factors $Q_{seismic}$ of specimens with different JRCs are calculated from Eq. (14) and shown in Fig. 13 and Table 2. In Fig. 13, the data in the dotted circle are the seismic quality factors of intact specimen G1,
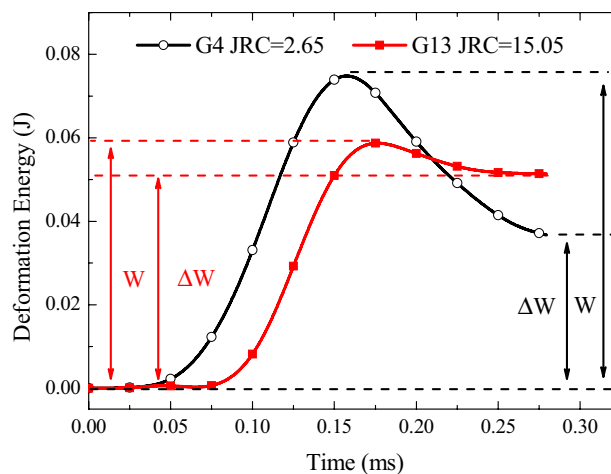
(a) G4, G13
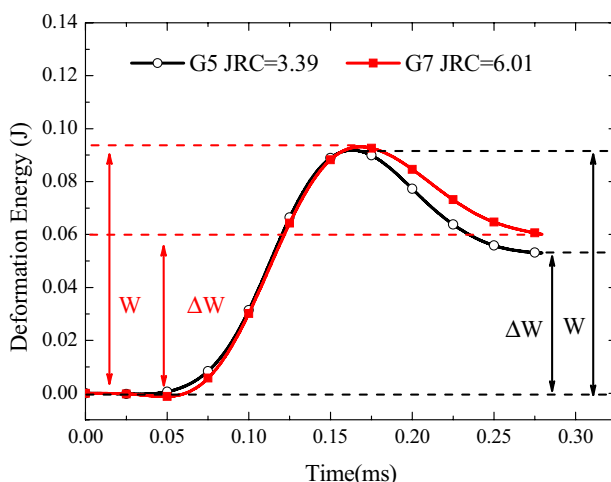
(b) G5, G7

(c) G9, G12

Fig. 12 Deformation energy of specimens

Table 2 The $Q_{seismic}$ values of the jointed specimens with different JRCs

Series number	JRC	W/J	$\Delta W/J$	$Q_{seismic}$	Mean value	Standard deviation
G1	0	0.2324	0.0554	26.34	27.62	1.1209
		0.1675	0.0374	28.10		
		0.1915	0.0423	28.43		
G2	0.78	0.0952	0.0512	11.68	12.77	1.5861
		0.0893	0.0385	14.59		
		0.1179	0.0616	12.04		
G3	1.69	0.0727	0.0396	11.52	11.40	1.2870
		0.0996	0.0595	10.53		
		0.0689	0.0343	12.62		
G4	2.65	0.0642	0.0406	9.94	10.95	1.6042
		0.084	0.0522	10.11		
		0.0748	0.0367	12.80		
G5	3.39	0.1109	0.0751	9.28	10.77	1.4385
		0.0918	0.0530	10.88		
		0.096	0.0496	12.15		
G6	4.62	0.0811	0.0524	9.73	9.84	0.2944
		0.0983	0.0642	9.62		
		0.1715	0.1059	10.18		
G7	6.01	0.0931	0.0601	9.74	8.87	0.7620
		0.0612	0.0448	8.58		
		0.0374	0.0283	8.30		
G8	7.37	0.1109	0.0777	8.97	9.23	0.2343
		0.0898	0.0606	9.31		
		0.092	0.0614	9.42		
G9	9.75	0.1506	0.1027	9.21	8.77	0.4128
		0.1052	0.0788	8.40		
		0.1452	0.1048	8.71		
G10	11.20	0.1075	0.0788	8.57	8.39	0.1837
		0.0999	0.0747	8.40		
		0.0984	0.0753	8.21		
G11	12.34	0.1084	0.0793	8.59	8.33	0.2245
		0.0750	0.0573	8.23		
		0.1025	0.0788	8.18		
G12	13.69	0.1606	0.1404	7.19	7.46	0.2631
		0.1003	0.0817	7.71		
		0.1056	0.0888	7.47		
G13	15.05	0.0587	0.0514	7.18	7.07	0.0945
		0.0564	0.0505	7.02		
		0.0544	0.0486	7.02		
G14	16.59	0.0701	0.0645	6.82	6.83	0.0596
		0.0512	0.0466	6.90		
		0.0965	0.0894	6.78		

while the data in the dotted box are the seismic quality factors of the jointed specimens with JRCs ranging from 0.78 to 16.59. The plot shows that the data in the dotted circle are obviously greater than the data in the dotted box. The mean value of $Q_{seismic}$ for intact specimen G1 is about 27.62, while the mean value of $Q_{seismic}$ for jointed specimen G2 is 12.77, which is the maximum mean value for all the jointed specimens. The seismic quality factor of intact specimen is significantly greater than that of jointed specimen, which indicates that the existence of joint has significant influence on the seismic quality factor of specimen. Figure 13 shows that the seismic quality factor of specimen is also affected by the JRC. For the jointed specimens with different JRCs, $Q_{seismic}$ monotonously declines with the increase of JRC.
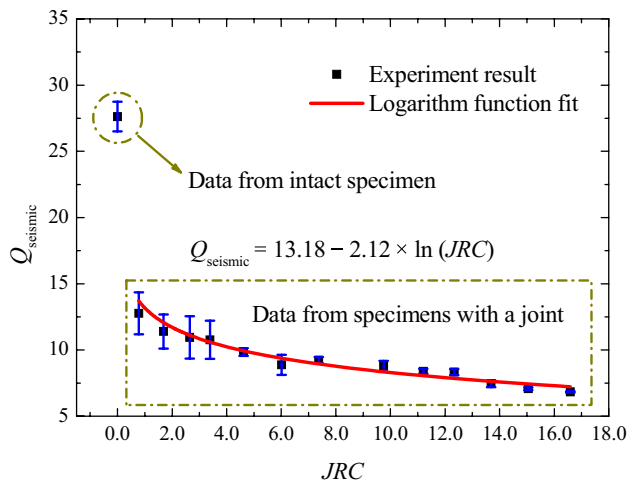
Fig. 13 The relationship between Q_{seismic} and JRC

Q_{seismic} drops a little faster in the small range of JRC and then turns to decrease smoothly in the great value of JRC. When the JRC decreases from 0.78 to 6.01, the value of Q_{seismic} drops from 12.77 to around 8.87, the value of Q_{seismic} drops about 30.54%. And when JRC decreases from 6.01 to 16.59, the value of Q_{seismic} drops from 8.87 to about 6.87, the decrease of Q_{seismic} is about 22.55%.

For the jointed specimens, the relation between Q_{seismic} and JRC was curved fitted using the least square regression method. The fitting curve shown in Fig. 13 is expressed as a logarithm function:

$$Q_{\text{seimic}} = 13.18 - 2.12 \times \ln(\text{JRC}). \tag{21}$$

5 Discussion

According to the definition of seismic quality factor, the wave energy dissipation is high during wave propagation across specimen with a low value of Q_{seismic}. The value of Q_{seismic} for a jointed specimen is obviously lower than that of intact specimen due to the existence of joint. The existence of joints results in energy dissipation and wave attenuation during wave propagation.

There are two possible reasons to cause wave energy dissipated during stress wave propagation across the jointed specimen: one is the friction between the joint surfaces and another is the damage of joint surfaces. To estimate whether the joint surfaces are damaged or not, the 3D digital images of joint rough surfaces were captured and compared to check the changes of joint surfaces before and after the SHPB tests, respectively. The 3D scanner was used and the two joint surfaces of specimens G9 and G14 with JRC 9.75 and 16.59, respectively, were chosen for the estimation.

The digital images of joint surfaces captured before and after the tests are shown in Fig. 14. The plot illustrates that

the joint surfaces geometry do not change in appearance after dynamic compression tests. This means the asperities of the joint surface are not crushed or cracked under the visual inspection. To further estimate the possible damage of joint surfaces, the differences of point height for the joint surface before and after tests are used to quantitatively measure the changes between the joint surfaces before and after the SHPB test.
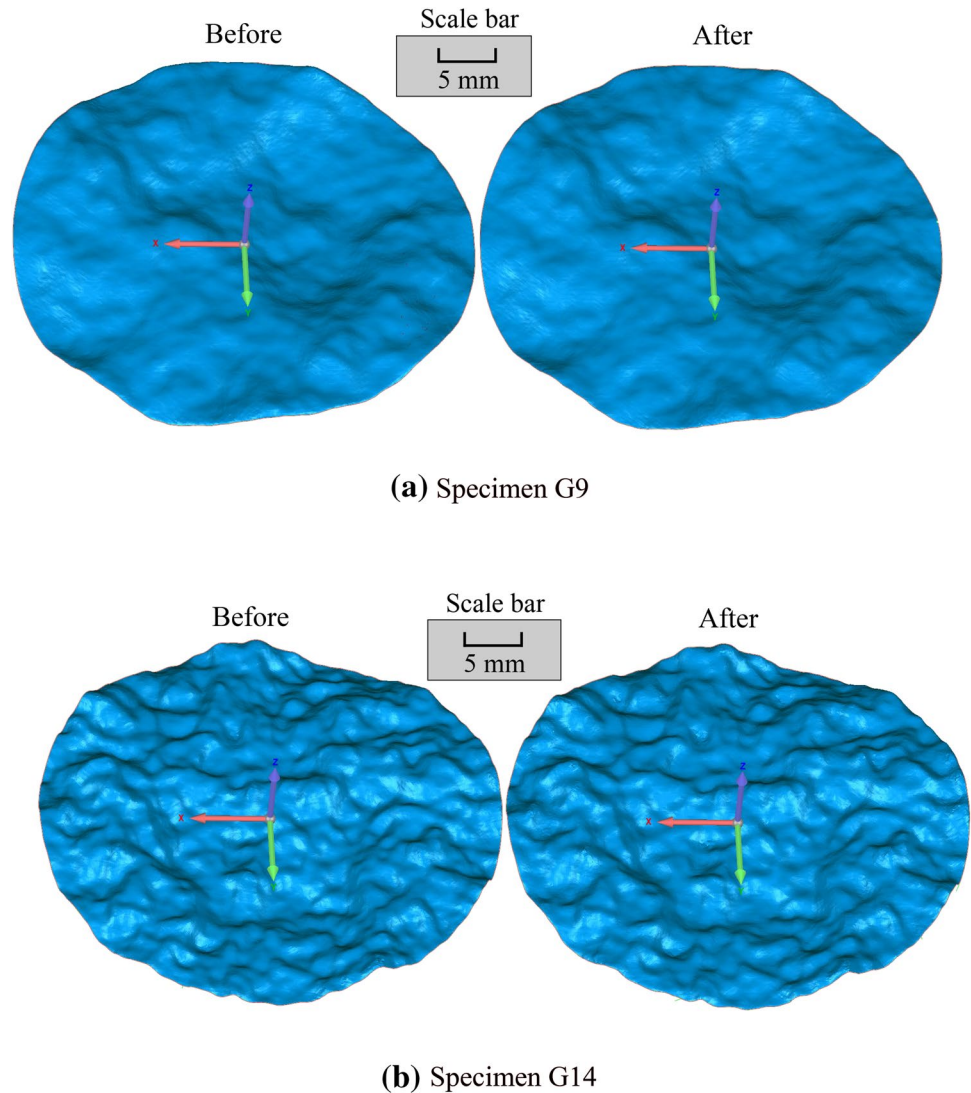
Figure 15 shows the changes in height for each joint surface before and after the tests. The differences of height are described as different colors in the picture, and darker color means greater changes in height. A larger difference of point height on the surface means the joint surface changes more after the test. Figure 15 shows that the maximum differences of point height are about 0.11 mm and 0.24 mm for the joint surfaces of specimen G7 and G12, respectively. The 3D digital image of each joint surface is consisted of 76,805 data points. Most of the differences of point height for the data points on the joint surfaces before and after tests are very small and range from −0.09 to 0.09 mm. In this range, there are about 99.95% data points on the joint surface of specimen G7 and about 98.45% data points for the joint surface of specimen G12. Figure 15 reveals that the joint surfaces captured after the SHPB test are almost the same as those before the test. Hence, the joint surfaces of specimen can be considered to be undamaged during the SHPB test. This indicates that the energy dissipated due to the joint should be caused by the friction between the joint surfaces but not by the damage of the joint surfaces.

6 Conclusions

The intension of this paper is to study the effect of joint surface topography, i.e. joint roughness coefficient (JRC), on the wave energy attenuation and the seismic quality factor of rock mass using the modified SHPB apparatus. In this study, a new approach is introduced to calculate the seismic quality factor Q_{seismic} based on stress wave energy. For the SHPB tests, this approach is more simple than the traditional approach which depends on stress–strain curve of specimen, and as valid as the traditional approach. Using the wave energy approach, Q_{seismic} of specimens with different JRCs is obtained.

The test result indicates that the joint roughness coefficient (JRC) has evident influence on the wave energy attenuation. The seismic quality factor decreases monotonously with the increase of joint roughness coefficient. When the joint surface is rougher, the seismic quality factor of specimen is lower. This indicates that a rougher joint results in more dissipation of wave energy. The seismic quality factor of the intact specimen is obviously higher than that of the specimen with joint. That is to say, the existence of joint
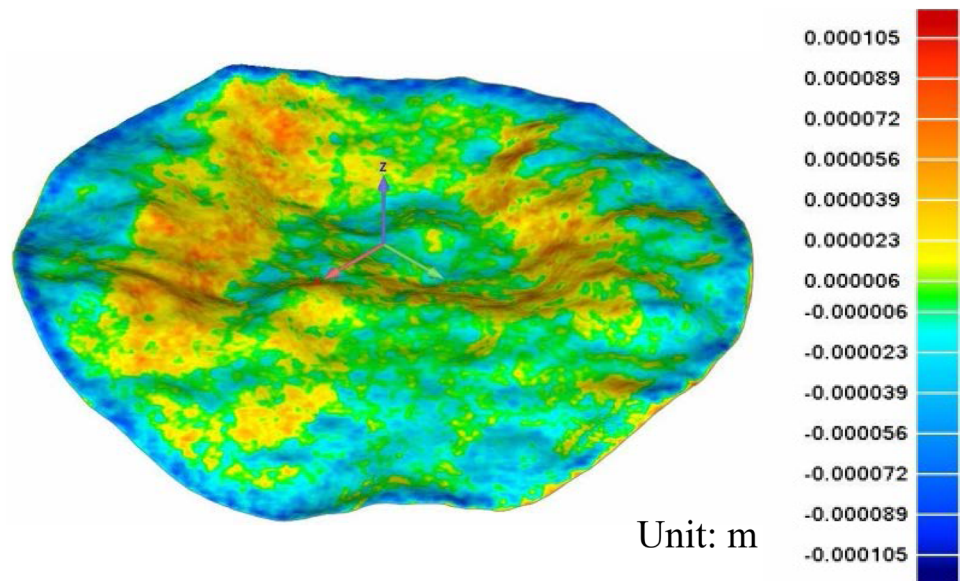
Fig. 14 The digital images for the joint surfaces of G9 and G14 before and after the tests
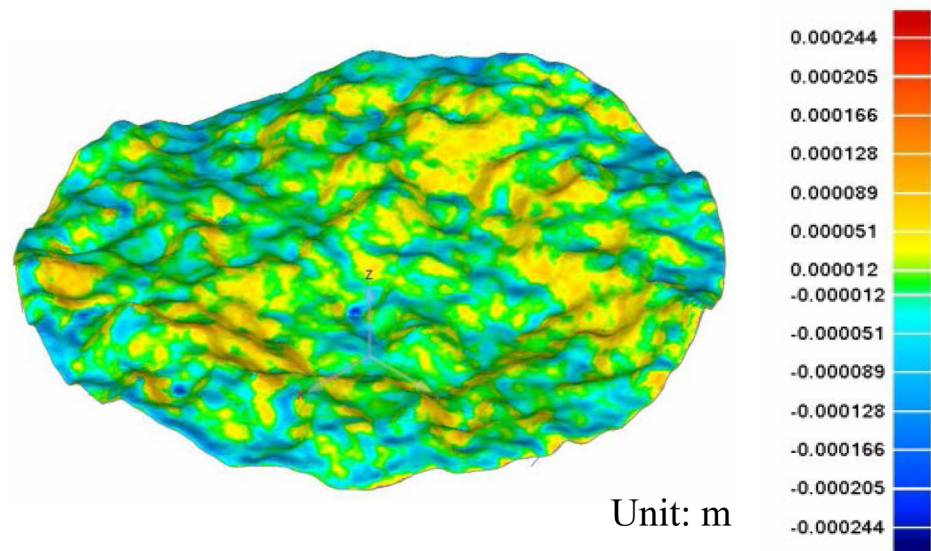

(a) Specimen G9

(b) Specimen G14

results in wave energy dissipation and has significant influence on the seismic quantity factor of specimen. It should be noted that the specimens adopted in the dynamic tests are made from gypsum plaster and binder, which are weaker than the most natural rocks in terms of elastic modulus. The rock in nature and the specimen material in the test have different elastic modulus, which results in different longitudinal wave velocities in the media but has no influence on the wave energy attenuation. In addition, due to the existence of binder, the viscosity of specimen must be higher than that of natural rock, which leads to more wave energy attenuation. So the seismic quality of specimens, Q_{seismic}, measured in this study is lower than that of natural rocks. But the viscosity does not affect the variation of seismic quality of specimen if the joint roughness is given. Hence, the relation between joint roughness coefficient and seismic quality factor of specimen is helpful to understand the energy attenuation during wave propagation across the joints with different surface morphology, and is also useful to predict the particle vibration of rock masses.

Fig. 15 The difference of point height for the joint surfaces of G9 and G14 before and after the tests (unit: m)

Unit: m

(a) Specimen G9

Unit: m

(b) Specimen G14

References

Aydan Ö (2017) ISRM book series 3: rock dynamics. CRC Press, London

Bacon C (1998) An experimental method for considering dispersion and attenuation in a viscoelastic Hopkinson bar. Exp Mech 38(4):242–249

Barton N, Choubey V (1977) The shear strength of rock joints in theory and practice. Rock Mech Rock Eng 10(1):1–54

Brown SR (1995) Simple mathematical model of a rough fracture. J Geophys Res Solid Earth 100(B4):5941–5952

Brown SR, Scholz CH (1986) Closure of rock joints. J Geophys Res Solid Earth 91(B5):4939–4948

Chen X, Li JC, Cai MF, Zou Y, Zhao J (2015) Experimental study on wave propagation across a rock joint with rough surface. Rock Mech Rock Eng 48(6):2225–2234

Chen X, Li JC, Cai MF, Zou Y, Zhao J (2016) A further study on wave propagation across a single joint with different roughness. Rock Mech Rock Eng 49(7):2701–2709

Fan LF, Wong L (2013) Stress wave transmission across a filled joint with different loading/unloading behavior. Int J Rock Mech Min Sci 60:227–234

Hopkins DL (2000) The implications of joint deformation in analyzing the properties and behavior of fractured rock masses, underground excavations, and faults. Int J Rock Mech Min Sci 37(1):175–202

Johnston DH, Toksoz MN, Timur A (1979) Attenuation of seismic waves in dry and saturated rocks: II. Mechanisms. Geophys 44(4):691–711

Knopoff L (1964) Q. Rev Geophys 2(4):645–654

Kolsky H (1963) Stress waves in solids. Dover Publications, New York

Li JC (2013) Wave propagation across non-linear rock joints based on time-domain recursive method. Geophys J Int 193(2):970–985

Li JC, Li NN, Li HB, Zhao J (2017) An SHPB test study on wave propagation across rock masses with different contact area ratios of joint. Int J Impact Eng 105:109–116

Mohd-Nordin MM, Song KI, Cho GC, Mohamed Z (2014) Long-wavelength elastic wave propagation across naturally fractured rock masses. Rock Mech Rock Eng 47(2):561–573

Ogilvie SR, Isakov E, Glover PWJ (2006) Fluid flow through rough fractures in rocks. II: A new matching model for rough rock fractures. Earth Planet Sci Lett 241(3):454–465

Perino A, Zhu JB, Li JC, Barla G, Zhao J (2010) Theoretical methods for wave propagation across jointed rock masses. Rock Mech Rock Eng 43(6):799–809

Pyrak-Nolte LJ, Myer LR, Cook NGW (1990) Transmission of seismic waves across single natural fractures. J Geophys Res Solid Earth Planet 95(B6):8617–8638

Wu W, Zhu JB, Zhao J (2013) Dynamic response of a rock fracture filled with viscoelastic materials. Eng Geol 160(12):1–7

Yang Z, Lo S, Di C (2001) Reassessing the joint roughness coefficient (JRC) estimation using Z_2. Rock Mech Rock Eng 34(3):243–251

Zhao J (1997a) Joint surface matching and shear strength part A: joint matching coefficient (JMC). Int J Rock Mech Min Sci 34(2):173–178

Zhao J (1997b) Joint surface matching and shear strength part B: JRC–JMC shear strength criterion. Int J Rock Mech Min Sci 34(2):179–185

Zhao J, Zhao XB, Cai JG (2006) A further study of P-wave attenuation across parallel fractures with linear deformational behaviour. Int J Rock Mech Min Sci 43(5):776–788

Zhu JB, Perino A, Zhao GF, Barla G, Li JC, Ma GW, Zhao J (2011) Seismic response of a single and a set of filled joints of viscoelastic deformational behaviour. Geophys J Int 186(3):1315–1330